

Supporting Information

Dipole-improved gating of azulene-based single-molecule transistors

Huanyan Fu,^{‡ab} Cong Zhao,^{‡a} Jie Cheng,^{‡c} Shuyao Zhou,^{‡b} Peizhen Peng,^c Jie Hao,^a
Zhirong Liu,^b Xike Gao,^{*c} Chuancheng Jia^{*ab} and Xuefeng Guo^{*ab}

Affiliations:

- Center of Single-Molecule Sciences, Institute of Modern Optics, Frontiers Science Center for New Organic Matter, College of Electronic Information and Optical Engineering, Nankai University, 38 Tongyan Road, Jinnan District, Tianjin 300350, P. R. China.
- Beijing National Laboratory for Molecular Sciences, National Biomedical Imaging Center, College of Chemistry and Molecular Engineering, Peking University, 292 Chengfu Road, Haidian District, Beijing 100871, P. R. China.
- Key Laboratory of Synthetic and Self-Assembly Chemistry for Organic Functional Molecules, Shanghai Institute of Organic Chemistry, University of Chinese Academy of Sciences, Chinese Academy of Sciences, Shanghai 200032, China.

[‡]These authors contributed equally to this work.

*Corresponding author. Email: guoxf@pku.edu.cn (XF. G.); jiacc@nankai.edu.cn (CC. J.); gaoxk@mail.sioc.ac.cn (XK. G.)

Contents

1. Molecular synthesis
2. Details of device fabrication and characterization
3. Theoretical calculations of transport properties
4. Single-molecule connection analyses
5. References

1. Molecular synthesis

1.1 General information

All reactions were performed under dry nitrogen atmosphere. Unless otherwise mentioned, all commercial reagents and solvents were obtained from chemical suppliers (Bide, Sinopharm, Energy, J&K, Macklin *etc.*) and used without further purification. Reactions were monitored by thin layer chromatography (TLC) on silica gel plates (GF254), and the flash column chromatography was carried out using 300-400 mesh silica gel. Nuclear magnetic resonance (NMR) spectra were recorded on a 400 MHz JEOL JMTC-400 or 500 MHz Avance Neo 600 NMR spectrometer at room temperature, ¹H NMR spectra were recorded at 400 MHz and chemical shifts are reported in ppm using residual deuterated solvent peak as reference (CDCl₃: δ 7.26). Data are reported as follows: chemical shift, multiplicity, coupling constant (*J* in Hz) and integration. The following abbreviations were used to explain the multiplicities: s = singlet, d = doublet, t = triplet, q = quartet, m = multiplet, br = broad. ¹³C NMR spectra were recorded at 100 MHz or 125 MHz and chemical shifts are reported in ppm relative to residual deuterated solvent peak (CDCl₃: δ 77.00). High-resolution mass spectrum (HRMS) were recorded on a Thermo Scientific Q Exactive HF Orbitrap-FTMS (fourier-transform mass spectrometry) in the electron spray ionization (ESI) mode or Bruker APEIII FTICRMS MALDI-TOF-MS. Infrared spectra were recorded on a NICOLET AVATAR 330 FT-IR (fourier-transform infrared) Spectrometer, and samples were scanned as neat liquids or in potassium bromide (KBr) salt plates.

1.2 Synthetic Procedures

Compounds **S1** and **S3** were synthesized from tropolone according to the literature.¹

Synthesis of 2,7-bis(2-bromoazulen-6-yl)-9,9-dioctyl-9H-fluorene (S3): 2,6-dibromoazulene **S1** (142.9 mg, 0.5 mmol), 2,2'-(9,9-dioctyl-9H-fluorene-2,7-diyl)bis(4,4,5,5-tetramethyl-1,3,2-dioxaborolane) **S2** (128.5 mg, 0.5 mmol), Pd(PPh₃)₄ (58 mg, 0.05 mmol) and silver carbonate (165.5 mg, 0.6 mmol) were charged in a Schlenck bottle. After evacuating and refilling with nitrogen over 3 times, 10 ml

oxygen-free tetrahydrofuran (THF) was added, and the mixture was allowed to stir at 70 °C for 24 h. After cooling to ambient temperature, the reaction was quenched with 50 mL H₂O and extracted with dichloromethane (DCM) (30 mL × 3). The combined organic layers were dried over anhydrous Na₂SO₄ and concentrated in vacuo. The crude product was purified by flash column chromatography by using petroleum ether (PE) / ethyl acetate (EA) (4:1, v/v) as eluent to give the product as a purple-red solid. Yield: 320 mg (81%). m.p. = 182 – 184 °C. ¹H NMR (400 MHz, CDCl₃) δ 8.33 (d, *J* = 10.1 Hz, 1H), 7.84 (d, *J* = 7.7 Hz, 1H), 7.70–7.61 (m, 1H), 7.55 (d, *J* = 10.1 Hz, 1H), 7.37 (s, 1H), 2.10 (d, *J* = 7.0 Hz, 1H), 1.10 (s, 5H), 0.80 (t, *J* = 6.7 Hz, 3H). MS (MALDI-TOF) calcd. for C₄₉H₅₃Br₂ [M+H]⁺: 799.25, found 801.40. The data are according with previous report.^[1]

Synthesis of 4,4'-((9,9-dioctyl-9H-fluorene-2,7-diyl)bis(azulene-6,2-diyl)dianiline

(**AM**): 2,7-bis(2-bromoazulen-6-yl)-9,9-dioctyl-9H-fluorene **S3** (320 mg, 0.4 mmol), (4-aminophenyl)boronic acid **S4** (219 mg, 1.6 mmol), Pd(PPh₃)₄ (46 mg, 0.04 mmol) and potassium carbonate (331 mg, 2.4 mmol) were charged in a Schlenk tube. After evacuating and refilling with nitrogen over 3 times, 6 ml degassed THF/H₂O (5:1, v/v) mixed solvent was added and the mixture was allowed to stir at 80 °C for 12 h. After cooling to room temperature, the reaction was quenched with 20 mL H₂O and extracted with DCM (20 mL × 3). The combined organic layers were dried over anhydrous Na₂SO₄ and concentrated in vacuo. The crude product was purified by flash column chromatography by using PE/DCM (20:1, v/v) as eluent to give the product as a yellow-green solid. Yield: 155 mg (47%). m.p. > 250°C. ¹H NMR (400 MHz, DMSO-*d*₆) δ 8.23 (d, *J* = 10.0 Hz, 4H), 7.93 (d, *J* = 7.6 Hz, 2H), 7.79 (d, *J* = 4.7 Hz, 4H), 7.76 (s, 2H), 7.68 (d, *J* = 7.9 Hz, 2H), 7.63 (s, 4H), 7.45 (d, *J* = 10.0 Hz, 4H), 6.68 (d, *J* = 8.1 Hz, 4H), 5.58 (s, 4H), 2.12 (s, 4H), 1.05 (d, *J* = 26.5 Hz, 24H), 0.71 (t, *J* = 6.8 Hz, 6H). ¹³C NMR (125 MHz, DMSO-*d*₆) δ 151.4, 150.5, 149.8, 147.2, 143.8, 140.0, 139.9, 132.9, 128.6, 127.5, 123.9, 123.2, 122.6, 120.5, 114.2, 113.1, 55.2, 31.1, 29.1, 28.5, 28.4, 23.4, 22.1, 13.9. FT-IR (film, cm⁻¹) ν_{max} 3372.3, 2923.0, 2580.4, 1617.0, 1604.7,

1570.6, 1544.0, 480.7, 1466.2, 1407.9, 1284.4, 1181.5, 821.3. HRMS (MALDI-TOF) calcd. for C₆₁H₆₅N₂ [M+H]⁺: 825.5142, found 825.5142.

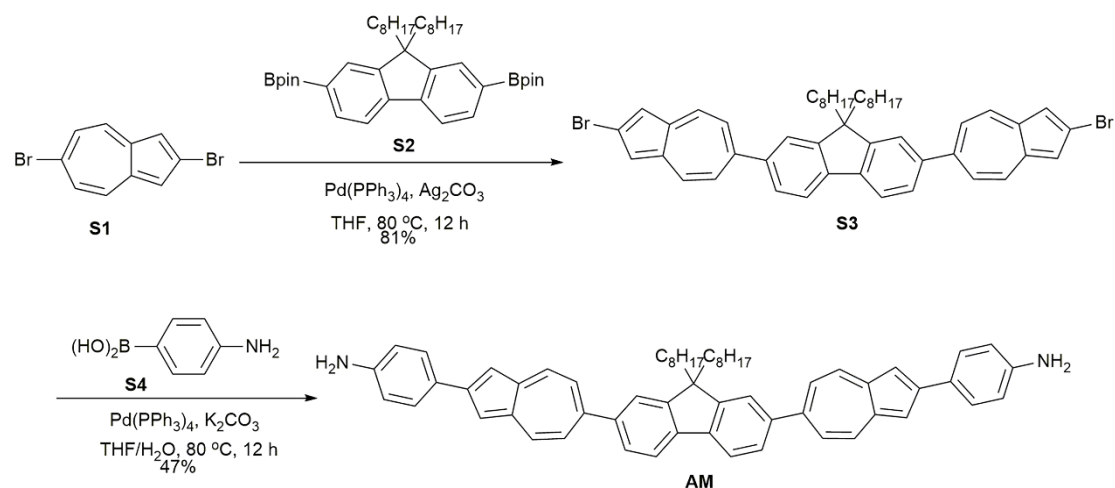


Fig. S1: Synthetic routes of AM

Synthesis of 6,6'-(9,9-dioctyl-9H-fluorene-2,7-diyl)bis(naphthalen-2-ol) (S6): 2,2'-(9,9-dioctyl-9H-fluorene-2,7-diyl)bis(4,4,5,5-tetramethyl-1,3,2-dioxaborolane) **S2** (1.35 g, 2 mmol), 6-bromonaphthalen-2-ol **S5** (1.34 g, 6 mmol), Pd(PPh₃)₄ (236 mg, 0.2 mmol), tetrabutylammonium bromide (13 mg, 0.04 mmol), potassium carbonate (1.1 g, 8 mmol) and 30 ml 1,4-dioxane/H₂O (4:1, v/v) mixed solvent were charged in a Schlenck bottle. Then the reaction mixture was allowed to bubble with nitrogen over 20 min and stirred at 80 °C for 18 h. After cooling to ambient temperature, the reaction was quenched with 50 mL H₂O and extracted with EA (30 mL × 3). The combined organic layers were dried over anhydrous Na₂SO₄ and concentrated in vacuo. The crude product was purified by flash column chromatography by using PE/EA (5:1, v/v) as eluent to give the product as a white solid. Yield: 734.8 mg (54%). Decomposed in air. ¹H NMR (400 MHz, CDCl₃) δ 8.06 (s, 2H), 7.90 – 7.78 (m, 8H), 7.74 – 7.65 (m, 4H), 7.21 (s, 2H), 7.17 (d, *J* = 8.8 Hz, 2H), 5.29 (s, 2H), 2.17 – 2.04 (m, 4H), 1.19 – 1.09 (m, 20H), 0.78 (t, *J* = 6.9 Hz, 10H). ¹³C NMR (100 MHz, CDCl₃) δ 153.6, 151.9, 140.1, 137.0, 133.9, 130.3, 129.4, 127.0, 126.6, 126.3, 125.7, 121.7, 120.2, 118.4, 109.5, 55.5, 40.6, 31.9, 30.2, 29.4, 29.3, 24.0, 22.7, 14.2. FT-IR (film, cm⁻¹) ν_{max} 3358.5, 2922.9, 2847.8, 1630.1, 1604.4, 1508.6, 1488.5, 1391.3, 1374.2, 1274.6, 1231.4, 1197.6,

1176.1, 115.08, 926.4, 881.4, 861.0, 800, 494.2, 472.7. HRMS (ESI) calcd. for $C_{49}H_{53}O_2$ [M-H]⁻: 673.4051, found: 673.4051.

Synthesis of (9,9-dioctyl-9H-fluorene-2,7-diyl)bis(naphthalene-6,2-diyl)bis(trifluoromethanesulfonate) (S7): 6,6'-(9,9-dioctyl-9H-fluorene-2,7-diyl)bis(naphthalen-2-ol) **S6** (533 mg, 0.79 mmol) were charged in a Schlenk bottle. After evacuating and refilling with nitrogen over 3 times, 15 mL DCM and 0.9 mL triethylamine (TEA) were added, then the mixture was allowed to stir in an ice-water bath. After the solid was dissolved, 0.53 mL trifluoromethanesulfonic anhydride was added dropwise via a syringe. After stirring in the ice-water bath for 1 h, the reaction was allowed to recover to ambient temperature and stirred overnight. The reaction was quenched with sat. $NaHCO_3$ in the ice-water bath and extracted with DCM (50 mL \times 3). The combined organic layers were dried over anhydrous Na_2SO_4 and concentrated in vacuo. The crude product was purified by flash column chromatography by using PE/EA (9:1, v/v) as eluent to give the product as a white solid. Yield: 422.8 mg (57%). ¹H NMR (400 MHz, $CDCl_3$) δ 8.17 (s, 2H), 8.10 – 7.92 (m, 6H), 7.87 (d, J = 7.9 Hz, 2H), 7.81 (d, J = 2.4 Hz, 2H), 7.74 (d, J = 7.8 Hz, 2H), 7.71 (s, 2H), 7.43 (dd, J = 9.0, 2.5 Hz, 2H), 2.23 – 2.03 (m, 4H), 1.11 (d, J = 11.1 Hz, 20H), 0.78 (t, J = 6.9 Hz, 10H). ¹³C NMR (100 MHz, $CDCl_3$) δ 152.1, 147.2, 140.6, 139.5, 132.8, 132.5, 130.9, 128.6, 127.7, 126.6, 125.7, 121.9, 120.5, 120.2, 119.2, 117.3, 55.6, 40.5, 31.9, 30.1, 29.3, 29.3, 23.9, 22.7, 14.2. ¹⁹F NMR (376 MHz, $CDCl_3$) δ -72.60. FT-IR (film, cm^{-1}) ν_{max} 2926.0, 2855.2, 1603.8, 1421.7, 1212.4, 1140.8, 1108.9, 961.1, 928.6, 886.8, 809.2, 718.8, 610.7, 505.1, 476.8.

Synthesis of 4,4'-((9,9-dioctyl-9H-fluorene-2,7-diyl)bis(naphthalene-6,2-diyl)dianiline) (NM): (9,9-dioctyl-9H-fluorene-2,7-diyl)bis(naphthalene-6,2-diyl)bis(trifluoromethanesulfonate) **S7** (282 mg, 0.3 mmol), 4-Aminophenylboronic acid hydrochloride **S8** (134 mg, 0.75 mmol), $Pd(PPh_3)_4$ (35 mg, 0.03 mmol), tetrabutylammonium bromide (2 mg, 0.006 mmol), potassium carbonate (248 mg, 1.8 mmol) and 5 ml 1,4-dioxane/ H_2O (4:1, v/v) mixed solvent were charged in a Schlenk

bottle. Then the reaction mixture was allowed to bubble with nitrogen over 20 min and stirred at 80 °C for 12 h. After cooling to ambient temperature, the reaction was quenched with 30 mL H₂O and extracted with EA (30 mL × 3). The combined organic layers were dried over anhydrous Na₂SO₄ and concentrated in vacuo. The crude product was purified by flash column chromatography by using PE/DCM (1:1, v/v) as eluent to give the product as an off-white solid. Yield: 196.3 mg (79%). ¹H NMR (400 MHz, CDCl₃) δ 8.12 (s, 2H), 8.02 (s, 2H), 7.97 (d, *J* = 8.5 Hz, 4H), 7.85 (d, *J* = 8.1 Hz, 4H), 7.79 – 7.73 (m, 4H), 7.72 (s, 2H), 7.60 (d, *J* = 8.4 Hz, 4H), 6.83 (d, *J* = 8.4 Hz, 4H), 3.79 (s, 4H), 2.19 – 2.03 (m, 4H), 1.12 (d, *J* = 13.6 Hz, 20H), 0.78 (t, *J* = 6.9 Hz, 10H). ¹³C NMR (100 MHz, CDCl₃) δ 152.0, 146.1, 140.2, 140.1, 138.7, 138.6, 133.1, 132.6, 131.4, 128.7, 128.6, 128.4, 126.4, 126.2, 125.9, 125.5, 124.3, 121.8, 120.3, 115.6, 55.5, 40.6, 31.9, 30.2, 29.4, 29.3, 24.0, 22.8, 14.2. FT-IR (film, cm⁻¹) *v*_{max} 3444.5, 3362.9, 3211.6, 3027.8, 2847.6, 1619.6, 1520.7, 1485.7, 1459.4, 1374.5, 1274.8, 1251.1, 1183.9, 884.5, 811.1. HRMS (ESI) calcd. for C₆₁H₆₅N₂ [M+H]⁺: 825.5142, found 825.5139.

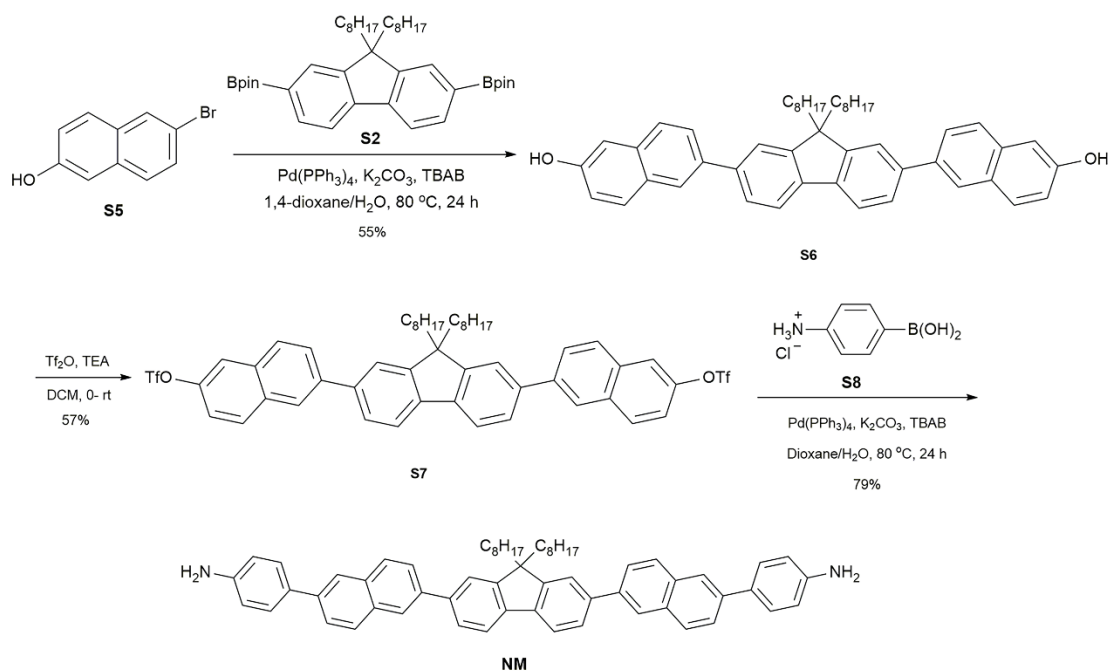


Fig. S2: Synthetic routes of NM

2. Details of device fabrication and characterization

The fabrication processes of graphene-based single-molecule transistors as shown in Figure 1a were listed as follows:

1. The high-quality monolayer graphene was grown on copper foil by chemical vapor deposition (CVD). Graphene transferred to silicon substrate with a 300 nm silicon oxide layer by etching. In order to more accurately fix the electrodes on the specific positions of the graphene strips, it is necessary to pattern marks first, then pattern the graphene strips, and finally pattern the electrodes. The marks and metal electrode arrays were patterned by photolithography and thermal evaporation. The mark is 8nm thick Cr and 40nm thick Au. The source/drain electrode is 8nm thick Cr and 60nm thick Au. In order to minimize the leakage current, the surface of source/drain electrode needs to cover 40nm thick SiO₂. The gate electrode is 8nm thick Cr, 40nm thick Au and 40nm thick Pt. The fabrication process is shown as Figure S3.

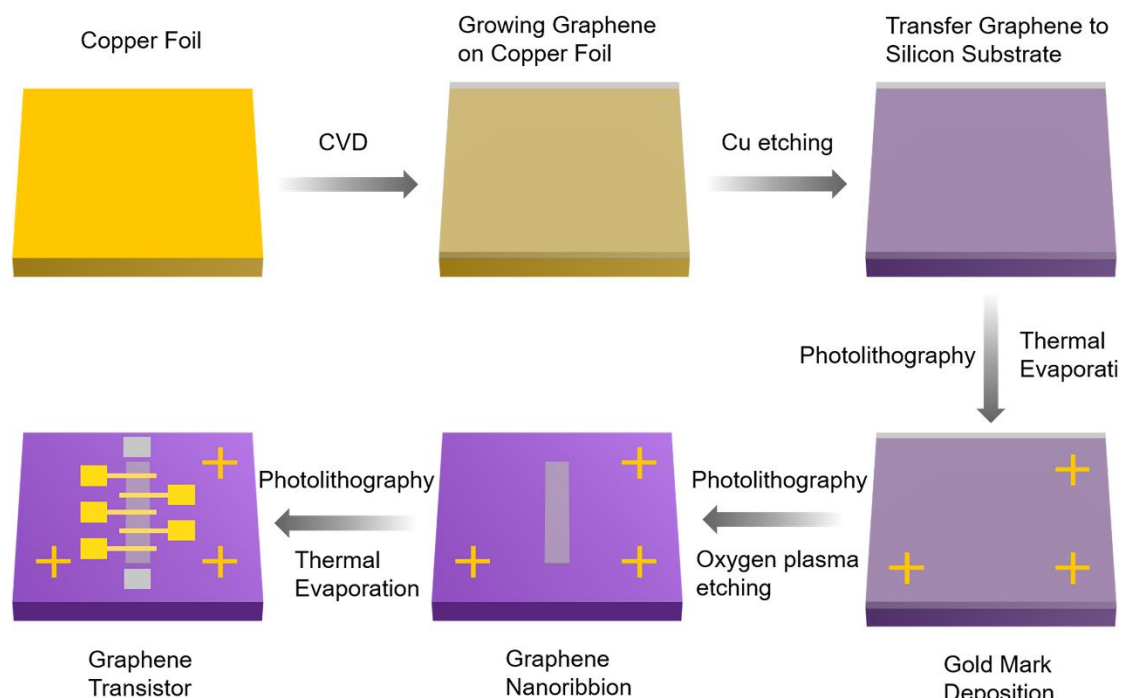


Fig. S3: The fabrication processes of graphene transistors.

2. The graphene nanoelectrode arrays were fabricated by a dash-line lithographic (DLL) method.² This process needs to use electron beam lithographic (EBL) technology, oxygen plasma etching technology and electroburning technology. The fabrication process shows as Figure S4.

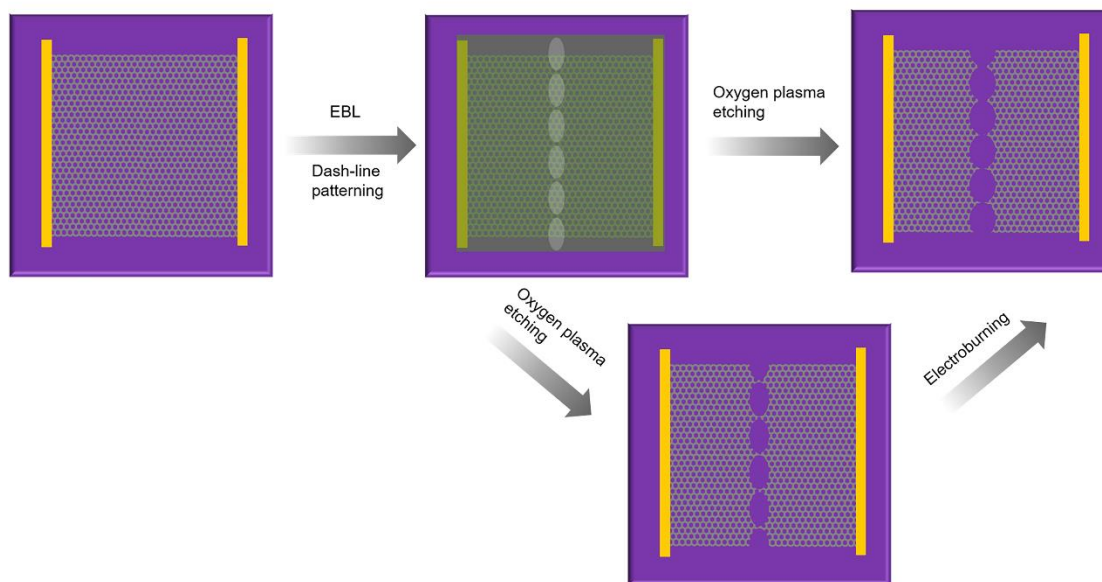


Fig. S4: The fabrication processes of graphene nanoelectrode arrays.

3. Molecules were connected to graphene point electrodes. First, the graphene devices and 1-ethyl-3-(3-dimethylaminopropyl) carbodiimide hydrochloride (EDCI) that is a well-known carbodiimide dehydrating/activating agent (~15mg) and molecule (~1mg AM or NM) were all added to a bottle. Then, the pyridine was added to bottle. The AM or NM molecule was dissolved in pyridine with the concentration about 10^{-4} M respectively. After two days, the device was removed, rinsed repeatedly with acetone and water and blow-dried with nitrogen. In the end, a small droplet ionic liquid was added to device, as shown in Figure S5.

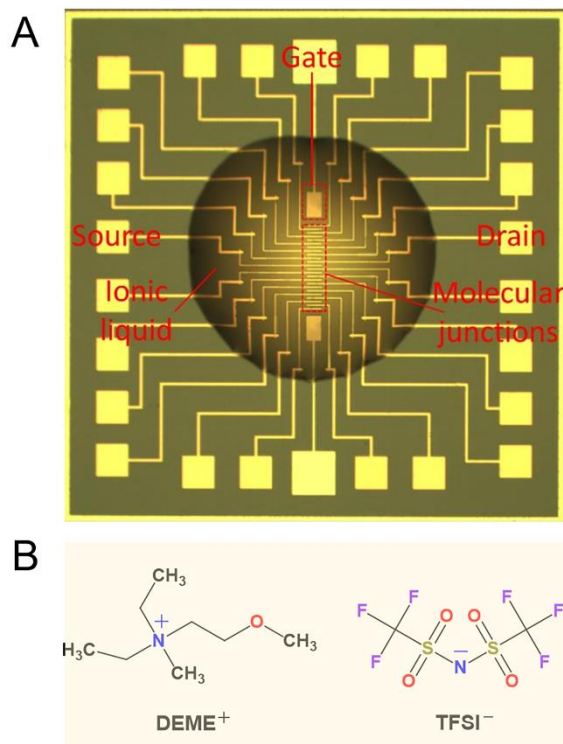


Fig. S5: (A) Optical image of single-molecule FET. Source, drain and gate electrodes were all covered with a small droplet of ionic liquid. (B) Molecular structures of the ionic liquid.

4. Device characterizations were carried out by utilizing an Agilent B1500A Semiconductor parameter meter and a TTPX (Lakeshore Company) with a liquid nitrogen cooling system. All the measurements were performed in vacuum, at 220 K. For the mapping of the current, the I - V curves at each fixed gate voltage were scanned with an interval of 10 mV step from -2 to 2 V.

3. Theoretical calculations of transport properties

The device structures were firstly relaxed in Gaussian 16 package using pm6 empirical method, as shown in Figure S6. For the calculation of the highest occupied molecular orbital (HOMO) and the lowest unoccupied molecular orbital (LUMO) energy levels for AM and NM molecules, we adopted the B3LYP/6-311+G (d, p) methodology implemented in the Gaussian 16 package,³ as shown in Figure S7.

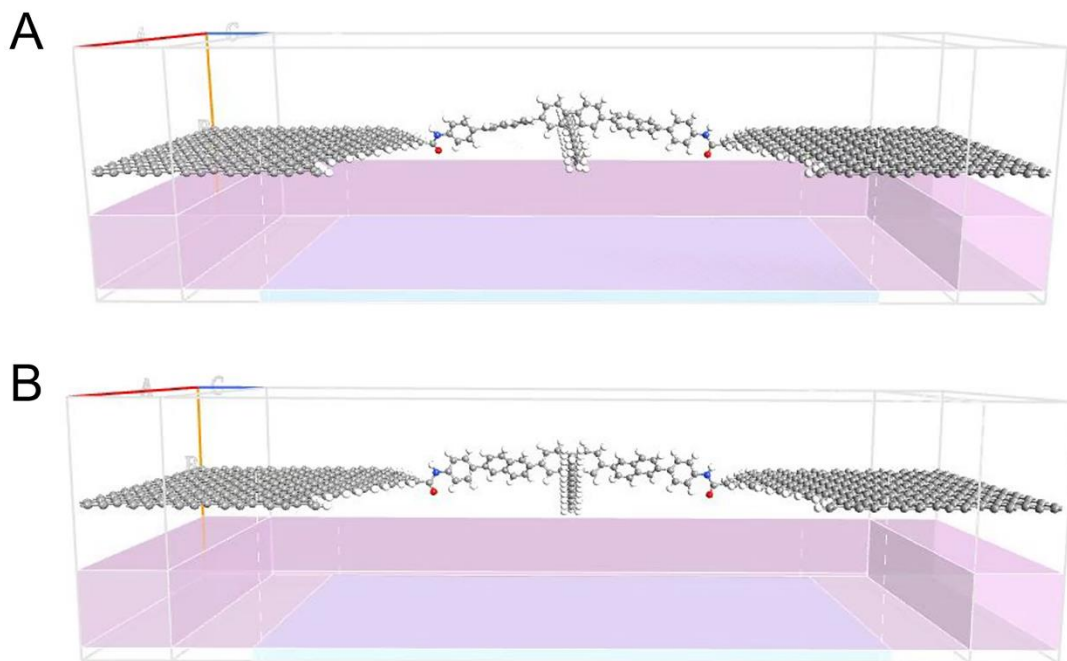


Fig. S6: (A) The geometry of an AM single-molecule FETs. (B) The geometry of an NM single-molecule FETs. They were both used to theoretical calculations.

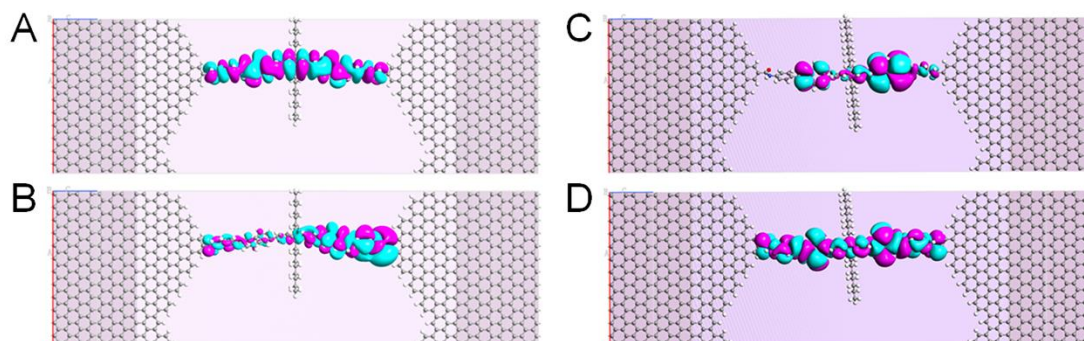


Fig. S7: Spatial distribution of (A) the perturbed highest occupied molecular orbit (p -HOMO) and (B) the perturbed lowest unoccupied molecular orbital (p -LUMO) for NM single-molecule junction; Spatial distribution of (C) the perturbed highest occupied molecular orbit (p -HOMO) and (D) the perturbed lowest unoccupied molecular orbital (p -LUMO) for AM single-molecule junction. They were all calculated at zero bias voltage and zero gate voltage.

Then the electronic transport simulations were performed using real-space non-equilibrium Green's function (NEGF) techniques implemented in the Atomistix Toolkit (ATK) package⁴⁻⁶. The general gradient approximation (GGA) functional with a double zeta plus polarization basis set and pseudoDojo pseudopotential were used. The energy cutoff for real-space mesh size was set to be 100 Hartree. The vacuum layer along b axis was set to be around 25 Å. Both electrodes were semi-infinite doped graphene. The scattering region consisted of the molecule and one surface layer on both sides. In the scattering region, we further placed an electrostatic gate and a dielectric region ($\epsilon \sim 14.5$)⁷ above the central molecule. The device self-consistent calculations were performed with a k-point mesh of $2 \times 1 \times 111$. Finally, the transmission spectra were computed with a k-point mesh of 24×1 .

To convince the influence of the dipole moment orientation on the properties of single-molecule FETs, the non-symmetric structure of AM-S (AM-NS, as shown in Fig. S8A) was calculated for comparison. As shown in Fig. S8B and Fig. S8C, the energy gap between p-HOMO and the Fermi level and the energy gap between p-HOMO and p-LUMO are similar for both systems. However, the transmission coefficient of AM-S around p-HOMO is higher than that of AM-NS, resulting in a higher on-state current of AM-S. Therefore, the on-off current ratio of AM-S with symmetric dipole moments is larger than that of AM-NS with non-symmetric dipole moments. From this, it can be speculated that the on-off current ratio is related to the direction of dipole moments.

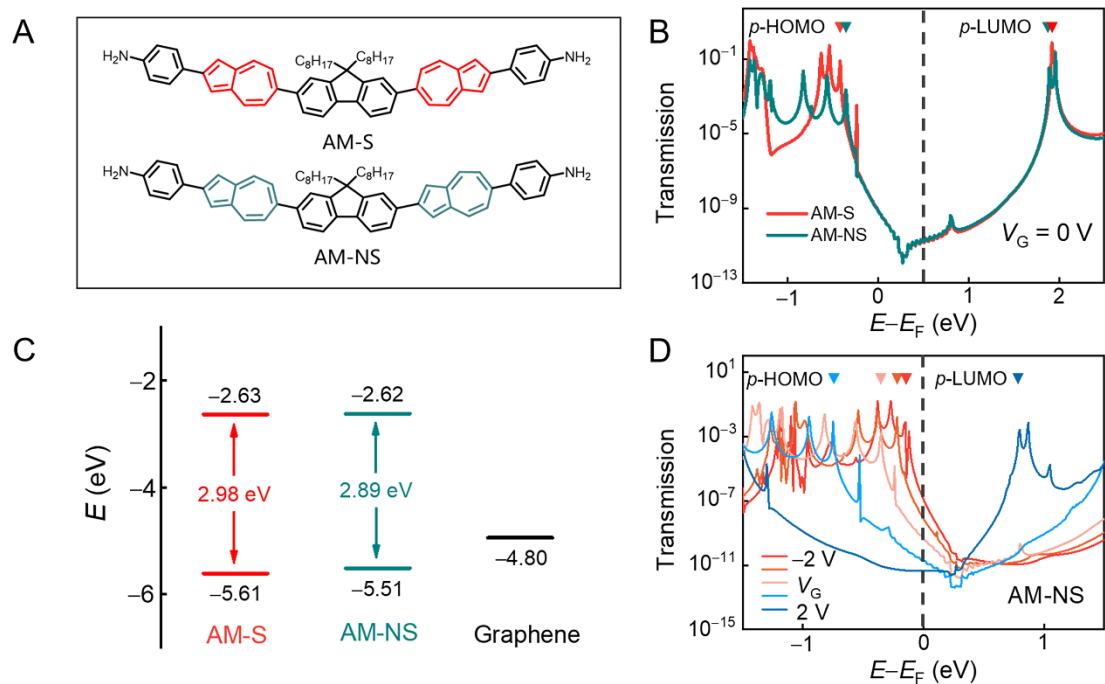


Fig. S8: The effect of the orientation of dipole moments to the on-off current ratio. (A) Molecular structures of AM-S and AM-NS with amine terminal groups at both ends. (B) Zero-bias transmission spectroscopies for AM-S-based and AM-NS-based single-molecule junctions. (C) Calculated molecular orbital energy levels of isolated molecules, and the Fermi level of graphene deduced from experiment results. (D) Gate-dependent zero-bias transmission spectroscopies for AM-NS-based single-molecule junctions at $-2 \text{ V} \leq V_G \leq 2 \text{ V}$ with a step of 1 V .

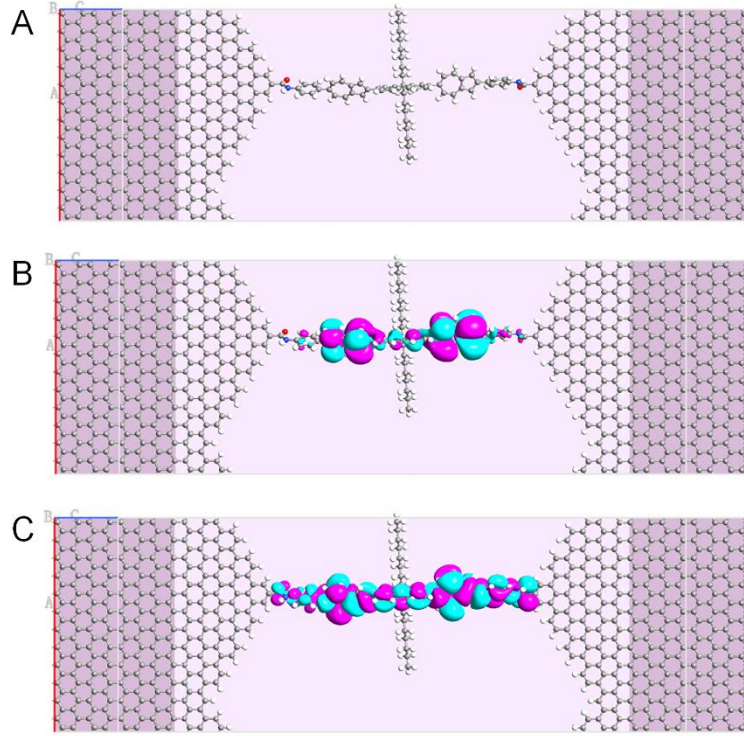


Fig. S9: Theoretical simulation results of AM-NS. (A) The geometry of an AM-NS single-molecule FETs. Spatial distribution of (B) the perturbed highest occupied molecular orbital (*p*-HOMO) and (C) the perturbed lowest unoccupied molecular orbital (*p*-LUMO) for AM-NS single-molecule junctions.

4. Single-molecule connection analyses

The number of junctions that contribute to charge transport can be carried out by calculating the probability of the reconnected devices with *n*-rejoined junctions (G_n):^{8,9}

$$G_n = \frac{m!}{n!(m-n)!} p^n (1-p)^{m-n} \quad n = 0, 1, 2 \dots, m$$

where *m* is the number of graphene point contact pairs (~210 in the current case) and *p* is the probability of the successful connection for a random junction. The device becomes conductive even if only one junction is reconnected. So, $Y_{\text{connection}}$ can be expressed by the formula:

$$Y_{\text{connection}} = 1 - G_0 = 1 - \frac{m!}{0!(m-0)!} p^0 (1-p)^m$$

Where G_0 is the probability of devices without any connected junctions. By using the $Y_{\text{connection}}$ values obtained from experiments, we can calculate the *p* values. And then

based on the p value, the ratios of single-junction or double junction devices to the overall reconnected devices [$G_n/(1-G_0)$] can be calculated. In our experiment, the average connection yields were found at ~24% for AM and ~22% for NM under optimized conditions. As the connection yield is among 20–30%, the ratio of single-junction devices to the overall reconnected devices are 82–89%. These results suggest that charge transport in these devices arises mainly in a single-molecule junction.

5. References

1. H. Gao, C. Ge, B. Hou, H. Xin and X. Gao, *ACS Macro Letters*, 2019, 8, 1360-1364.
2. Y. Cao, S. Dong, S. Liu, L. He, L. Gan, X. Yu, M. L. Steigerwald, X. Wu, Z. Liu and X. Guo, *Angew Chem Int Ed Engl*, 2012, 51, 12228-12232.
3. M. J. Frisch, G. W. Trucks, H. B. Schlegel, G. E. Scuseria, M. A. Robb, J. R. Cheeseman, G. Scalmani, V. Barone, G. A. Petersson, H. Nakatsuji, X. Li, M. Caricato, A. V. Marenich, J. Bloino, B. G. Janesko, R. Gomperts, B. Mennucci, H. P. Hratchian, J. V. Ortiz, A. F. Izmaylov, J. L. Sonnenberg, D. Williams-Young, F. Ding, F. Lipparini, F. Egidi, J. Goings, B. Peng, A. Petrone, T. Henderson, D. Ranasinghe, V. G. Zakrzewski, J. Gao, N. Rega, G. Zheng, W. Liang, M. Hada, M. Ehara, K. Toyota, R. Fukuda, J. Hasegawa, M. Ishida, T. Nakajima, Y. Honda, O. Kitao, H. Nakai, T. Vreven, K. Throssell, J. A. Montgomery, Jr., J. E. Peralta, F. Ogliaro, M. J. Bearpark, J. J. Heyd, E. N. Brothers, K. N. Kudin, V. N. Staroverov, T. A. Keith, R. Kobayashi, J. Normand, K. Raghavachari, A. P. Rendell, J. C. Burant, S. S. Iyengar, J. Tomasi, M. Cossi, J. M. Millam, M. Klene, C. Adamo, R. Cammi, J. W. Ochterski, R. L. Martin, K. Morokuma, O. Farkas, J. B. Foresman, and D. J. Fox, *Gaussian 16, Revision C.01* (Gaussian Inc., 2019).
4. M. Brandbyge, J.-L. Mozos, P. Ordejón, J. Taylor and K. Stokbro, *Physical Review B*, 2002, **65**, 165401.
5. J. Taylor, H. Guo and J. Wang, *Physical Review B*, 2001, **63**, 245407.
6. S. Smidstrup, T. Markussen, P. Vancraeyveld, J. Wellendorff, J. Schneider, T. Gunst, B. Verstichel, D. Stradi, P. A. Khomyakov, U. G. Vej-Hansen, M. E. Lee, S. T. Chill, F. Rasmussen, G. Penazzi, F. Corsetti, A. Ojanpera, K. Jensen, M. L. N. Palsgaard, U. Martinez, A. Blom, M. Brandbyge and K. Stokbro, *J Phys Condens Matter*, 2020, **32**, 015901.
7. F. Wang, P. Stepanov, M. Gray, C. N. Lau, M. E. Itkis and R. C. Haddon, *Nano Lett*, 2015, **15**, 5284-5288.
8. H. Wen, W. Li, J. Chen, G. He, L. Li, M. A. Olson, C.-H. Sue, J. F. Stoddart, X. Guo, *Sci. Adv.* **2016**, 2, e1601113.
9. N. Xin, C. Jia, J. Wang, S. Wang, M. Li, Y. Gong, G. Zhang, D. Zhu, X. Guo, *J. Phys. Chem. Lett.* **2017**, 8, 2849–2854.